AGU PUBLICATIONS

JGR

Journal of Geophysical Research: Atmospheres

RESEARCH ARTICLE
10.1002/2017JD027110

Key Points:
- Model simulations of solar geoengineering show a decrease in summer heat extremes relative to simulations with greenhouse warming
- Changes in soil moisture play a key role in the regional response to solar geoengineering
- Regional land surface hydrology exhibits trends over time that impact the variability response as the model adjusts to solar geoengineering

Supporting Information:
- Supporting Information S1

Correspondence to:
K. Dagon,
kdagon@fas.harvard.edu

Citation:
Dagon, K., & Schrag, D. P. (2017). Regional climate variability under model simulations of solar geoengineering. *Journal of Geophysical Research: Atmospheres*, *122*, 12,106–12,121. https://doi.org/10.1002/2017JD027110

Received 10 MAY 2017
Accepted 13 OCT 2017
Accepted article online 19 OCT 2017
Published online 20 NOV 2017

Regional Climate Variability Under Model Simulations of Solar Geoengineering

Katherine Dagon[1] **and Daniel P. Schrag**[1]

[1]Department of Earth and Planetary Sciences, Harvard University, Cambridge, MA, USA

Abstract Solar geoengineering has been shown in modeling studies to successfully mitigate global mean surface temperature changes from greenhouse warming. Changes in land surface hydrology are complicated by the direct effect of carbon dioxide (CO_2) on vegetation, which alters the flux of water from the land surface to the atmosphere. Here we investigate changes in boreal summer climate variability under solar geoengineering using multiple ensembles of model simulations. We find that spatially uniform solar geoengineering creates a strong meridional gradient in the Northern Hemisphere temperature response, with less consistent patterns in precipitation, evapotranspiration, and soil moisture. Using regional summertime temperature and precipitation results across 31-member ensembles, we show a decrease in the frequency of heat waves and consecutive dry days under solar geoengineering relative to a high-CO_2 world. However in some regions solar geoengineering of this amount does not completely reduce summer heat extremes relative to present day climate. In western Russia and Siberia, an increase in heat waves is connected to a decrease in surface soil moisture that favors persistent high temperatures. Heat waves decrease in the central United States and the Sahel, while the hydrologic response increases terrestrial water storage. Regional changes in soil moisture exhibit trends over time as the model adjusts to solar geoengineering, particularly in Siberia and the Sahel, leading to robust shifts in climate variance. These results suggest potential benefits and complications of large-scale uniform climate intervention schemes.

Plain Language Summary Climate change is a difficult problem and will likely require a wide range of solutions. The use of intentional climate interventions, also called solar geoengineering, could help combat the worst effects of climate change. Solar geoengineering refers to techniques that decrease the amount of sunlight reaching the Earth's surface in order to cool the planet. While this method may be helpful in some ways, we also need to understand the risks or any unintended consequences. In this work we focus on the potential impacts of solar geoengineering on extreme heat events, such as heat waves. We use a climate model to study how the frequency of these events is affected by solar geoengineering and compare with how future climate change impacts extremes. Our results show that solar geoengineering produces fewer extreme heat events than the future with global warming. However, some places show an increase in extremes relative to the climate of today. Finally, we find that water stored in the soils is an important factor in determining the local response of extreme heat events to solar geoengineering.

1. Introduction

Solar geoengineering has been proposed as a method of counteracting climate change through albedo modification (e.g., Crutzen, 2006; Keith & MacMartin, 2015; Rasch et al., 2008; Shepherd et al., 2009). Decreasing incoming sunlight can help compensate for the increase in longwave radiation from greenhouse gases such as carbon dioxide (CO_2). Previous climate modeling studies have shown that globally averaged surface warming from increases in atmospheric CO_2 concentration can be roughly compensated by spatially uniform reductions in the solar constant (Caldeira & Wood, 2008; Kravitz, Caldeira, et al., 2013). Similar studies have shown that this compensation also leads to a decrease in global annual mean precipitation (e.g., Bala et al., 2008; Dagon & Schrag, 2016; Kravitz, Rasch, et al., 2013; McCusker et al., 2012; Niemeier et al., 2013; Ricke et al., 2010; Tilmes et al., 2013). This phenomenon has been observed following large volcanic eruptions, when aerosol surface cooling reduces the latent heat flux of water vapor to the atmosphere and weakens the global hydrologic cycle (Gillett et al., 2004; Iles et al., 2013; Trenberth & Dai, 2007). Changes in shortwave forcing such as solar variability or volcanic eruptions have also been shown to be more effective in driving precipitation changes than the equivalent CO_2 forcing (Allen & Ingram, 2002; O'Gorman et al., 2012). Evaporation is expected to decrease under solar geoengineering because latent heat flux will respond

more strongly to changes in shortwave radiation than changes in longwave radiation (Andrews et al., 2009; Bala et al., 2010; Cao et al., 2012; Curry et al., 2014; Dagon & Schrag, 2016; Kleidon & Renner, 2013; Tilmes et al., 2013).

An additional factor contributing to the hydrologic response to solar geoengineering is the interaction between vegetation and climate. Changes in CO_2 alter the physiology of plants including through stomatal closure (Betts et al., 2007; Doutriaux-Boucher et al., 2009; Lammertsma et al., 2011), which leads to changes in transpiration, or the water flux from vegetation to the atmosphere (Field et al., 1995; Franks et al., 2013; Lee et al., 2012; Sellers et al., 1996). Changes in transpiration alter plant water use efficiency (Swann et al., 2016), defined as the ratio of photosynthesis to evapotranspiration (ET). Dagon and Schrag (2016) demonstrate that solar geoengineering has similar global and regional impacts on terrestrial water cycling. When solar geoengineering is modeled as a decrease in incoming solar radiation to compensate surface temperature changes from increased CO_2, the CO_2-induced stomatal closure is augmented by the decrease in solar radiation, leading to further decreases in ET (Dagon & Schrag, 2016). Furthermore, changes in ET can affect temperature and precipitation variability through soil moisture feedbacks (Seneviratne et al., 2010). This relationship explains the connection between low soil moisture availability and extreme heat events demonstrated in modeling and observational studies (Berg et al., 2016; Fischer et al., 2007, 2012; Hirschi et al., 2011; Lorenz et al., 2010; Miralles et al., 2014; Mueller & Seneviratne, 2012; Teuling et al., 2013).

Many studies have analyzed the impact of solar geoengineering on mean climate changes, and there is a growing effort to focus on climate extremes, as understanding and predicting the consequences of extreme events and their effects on humans and the environment is of great importance to society (Intergovernmental Panel on Climate Change (IPCC), 2012). Tilmes et al. (2013) analyze global distributions of precipitation under the context of standardized geoengineering experiments and find that the probability of extreme precipitation events is decreased, though they base their analysis on a multimodel mean. Using the same model intercomparison, Curry et al. (2014) find that solar geoengineering leads to smaller changes in mean, variance, and skewness of temperature and precipitation anomalies than the comparable high-CO_2 scenario, but that it is more effective in mitigating extreme temperatures than extreme precipitation. These results are again in the context of a multimodel ensemble average. Another study by Aswathy et al. (2015) uses an average of three models to contrast multiple solar geoengineering techniques and their effects on mean and extreme temperature. They find that the high tails of the temperature distribution change less in the geoengineering schemes relative to the Representative Concentration Pathway 4.5 scenario. Wilhelm et al. (2015) investigate climate engineering by altering model land surface albedo and show a cooling of hot extremes in northern midlatitudes, though they use only one model realization for each albedo perturbation. Though not in the context of solar geoengineering, previous work has explored large ensembles of multiple climate models (IPCC, 2013) and a single model (Barnett et al., 2006; Clark et al., 2006; Deser et al., 2012; Fischer et al., 2013; Kay et al., 2015) to study the response of extremes to climate change. These findings demonstrate that there is potential for solar geoengineering to alter climate variability, but there is a need for studies that utilize large ensembles to better capture the shifts in variance simulated in climate models. To the best of our knowledge, no study has examined changes in daily regional temperature and precipitation variability and the frequency of extreme events under solar geoengineering across multiple large ensembles of simulations from a single climate model.

In this work, we shift the focus from the ensemble mean as a projection of future climate and instead concentrate on discrete ensemble members and view them as individual realizations for a given boreal summer. This method is analogous to work on the statistics of tropical cyclone formation in Emanuel et al. (2006). Our approach examines the effect of solar geoengineering on daily regional summertime temperature and precipitation variability in the Northern Hemisphere using multiple large ensembles from a coupled atmosphere-land model with a slab ocean. We first create an ensemble of control simulations to learn about the statistics of boreal summer climate variability in the model, including seasonal-scale heat waves and persistent low precipitation events. We then repeat the ensemble member simulations with a decrease in the solar constant and an increase in carbon dioxide to mimic solar geoengineering and compare the resulting statistics. We also include an ensemble with the climate of a doubled CO_2 world, to compare solar geoengineering to a high greenhouse gas emissions scenario. Though our model parameterization of solar geoengineering is not reflective of a realistic scenario for implementation (e.g., Keith & MacMartin, 2015), we choose this approach to better understand impacts on variance. Instead of designing a policy relevant

scenario, we utilize model simulations that mitigate global temperatures from a doubling of CO_2 to learn about mechanisms related to climate variability and extremes. By comparing scenarios that have the same global mean temperature, and thus the same net energy balance, we are able to gain insight on model-induced mechanisms that affect regional variance.

We recognize that the model does not sample the complete range of climate variance and weather patterns. Variability in sea surface temperature and sea ice extent can have impacts on heat waves through a variety of mechanisms (e.g., Cohen et al., 2014; McKinnon et al., 2016), and these features are not fully captured here due to the limitations of a slab ocean model. However, our approach does not require the model to accurately depict real world variability. We focus on the intrinsic change in simulated variability, given what the model generates as a set of possible climates. Comparing the variance between ensembles with and without solar geoengineering allows us to learn about the mechanisms that cause changes in extremes at a regional scale. Supported by the underlying physics of the model, these results help improve understanding of potential real world mechanisms related to shifts in regional climate variability under solar geoengineering.

2. Methods

Here we use the Community Earth System Model, version 1.2.2 (CESM1.2.2), a coupled climate model developed by the National Center for Atmospheric Research (NCAR). We couple an atmospheric general circulation model (CAM4) to a dynamic land surface model (CLM4.5). CAM4 uses a finite volume dynamical core to solve the equations of motion on a sphere (Neale et al., 2010). We also couple the atmospheric model to a slab ocean model (SOM) with a thermodynamic sea ice model (Bitz et al., 2012). Prescribed mixed layer depths and surface heat fluxes for the SOM are derived from a fully coupled simulation. Use of a slab ocean implies that the model will not fully resolve ocean dynamics, though this option provides simplicity and computational advantages. We run the model with a horizontal resolution of 0.9° in latitude and 1.25° in longitude, with 26 vertical levels in the atmosphere. The model default value for atmospheric CO_2 concentration is increased from 367 to 400 parts per million (ppm) to match present-day values. All other greenhouse gas and aerosol concentrations are fixed at year 2000 values.

CLM4.5 separates grid cells into land surface type and simulates vertical moisture transport in a multilayer soil column model (Oleson et al., 2013). Vegetated land units are further partitioned into at most 15 plant functional types (PFT) plus bare ground. Evaporative fluxes are a weighted averaged over all the PFT present in each land unit. Here we prescribe vegetation distributions as well as leaf and stem area indices by satellite observations (Bonan et al., 2002). Soil hydrology in the model is represented by a 50 m depth column divided into 10 soil layers and 5 bedrock layers, the latter of which are hydrologically inactive (Lawrence et al., 2011). The soil layers span a depth of 3.8 m, with more layers near the surface where the soil water gradient is strong (Oleson et al., 2013). Soil moisture observations are limited; CLM has demonstrated skill in reproducing temporal variability of specific observations, though biases in surface soil moisture persist (Bi et al., 2016; Li et al., 2007).

We use this modeling framework to spin up the model for 30 years, after which the model climate has reached equilibrium based on interannual variability and linear trends of global average temperature and top of the atmosphere energy balance (Figures S1 and S2 and Table S1). We continue the model spin-up for five additional months, finishing at the end of May in the 31st model year. We then run the model with daily resolution output for the remainder of the 31st year and an additional 30 years to generate an ensemble of 31 members by sampling each boreal summer (June–August). This first ensemble, *Control*, represents a continuation of the spin-up with unperturbed climate. This method of sampling generates sufficient variability in the resulting model land surface temperature (Figure S3).

The second ensemble, *SolarGeo*, includes an instantaneous doubling of the CO_2 concentration to 800 ppm and a 2.2% decrease in the solar constant globally at all times. A reduction in solar radiation by this amount is sufficient to offset warming from a doubling of CO_2 in this model (Dagon & Schrag, 2016; Kravitz et al., 2015). After we impose solar geoengineering, we run for an additional 10 years of spin-up in order to allow the model to adjust to the solar geoengineering perturbation. Very little change in global mean temperature is observed in the 10 years after imposing solar geoengineering, further demonstrating that the reduction in solar radiation is sufficient to compensate climate changes from a doubling of CO_2 (Figure S1). The 31

ensemble members are generated starting on June 1 of the 42nd model year by completing the remainder of this year with daily resolution output and continuing the solar geoengineering run for 30 years to sample each summer.

We also generate a doubled CO_2 ensemble, *2xCO₂*, to understand the climate response to greenhouse gas warming and provide an additional comparison with solar geoengineering. This ensemble uses the same slab ocean forcing as the previous ensembles but starts from a different 30 year spin-up simulation in order for the model to equilibrate to a higher CO_2 concentration of 800 ppm (Figures S1 and S2). The 31 ensemble members are then generated starting on June 1 of the 31st model year, following the same procedure as the Control ensemble. All ensemble member simulations consist of daily mean output for 3 months through the end of boreal summer (June–August).

Caveats to our modeling framework are similar to what is reported in Dagon and Schrag (2016), including the parameterization of solar geoengineering as a fixed decrease in the solar constant instead of explicitly parameterizing aerosols in the stratosphere. While changes in incoming shortwave radiation are an approximation for how solar geoengineering might impact the surface energy budget, stratospheric chemistry and dynamics altered by the presence of aerosols will have downstream effects on climate variability, ozone, and ultraviolet radiation, which will in turn impact vegetation. Furthermore, decreases in ozone from the decrease of chlorofluorocarbons in the stratosphere have been shown to affect surface climate (Marsh et al., 2013), and these changes are not included here. Other model limitations include the lack of simulating the effect of diffuse radiation from an aerosol layer (Xia et al., 2016), and the approximation of nondynamical vegetation distributions, nutrient cycling, and land use change.

3. Results

3.1. Ensemble Means

In the Northern Hemisphere, the ensemble mean June–August (JJA) mean temperature response from solar geoengineering overcools at low latitudes, optimizes at midlatitudes, and undercools at high latitudes, relative to the Control ensemble mean (Figure 1a). The spatial variability of changes in daily mean surface air temperature (T_{mean}) is driven primarily by changes in daily maximum temperature (T_{max}) rather than changes in daily minimum temperature (T_{min}) (Figures 1b and 1c). Areas of increase in T_{max} are located over northern Canada, northern Europe, and Asia. T_{max} decreases over the central U.S., northern Africa, southern Europe, the Middle East, and central Asia. There is also a decrease in the pole-to-equator temperature gradient, as shown in Figure 2. This decrease is evident in all temperature values but most pronounced for T_{max}. The temperature gradient shows a weakening at the northernmost latitudes, due to the lack of land area and the influence of Arctic sea ice.

Ensemble mean JJA mean rainfall generally decreases in the Northern Hemisphere under solar geoengineering relative to the Control ensemble, except in Central America, northern Africa, and the Middle East (Figure 3a). ET also decreases throughout much of the Northern Hemisphere, with some localized increases in similar places where precipitation increases (Figure 3b). The difference between mean precipitation and evapotranspiration (P-ET) is shown in Figure 3c. There are regions where P-ET increases despite a decrease in precipitation (e.g., the eastern U.S.), because the local decrease in ET exceeds the decrease in precipitation. Changes in soil moisture are coupled with changes in precipitation and ET, with soils becoming drier as P-ET decreases and wetter as P-ET increases under solar geoengineering (Figure 3d). There is large spatial variability in the response, though the northern U.S., India, and northern Europe stand out as regions of decrease in JJA mean soil moisture of the top 10 cm. Soil moisture increases in the southeast U.S., northern Africa, the Middle East, and most of Asia, with some additional decreases in high northern latitudes (e.g., Siberia).

Solar geoengineering globally cools the land surface, relative to the $2xCO_2$ ensemble mean surface air temperature (Figure S4a). There are some regions where the magnitude of the cooling is lower, including the southeastern U.S. and India. In those regions T_{max} cools less than T_{min}, implying that changes in minimum temperature contribute more to mean surface cooling (Figures S4b and S4c). Precipitation and evapotranspiration over land generally decrease under solar geoengineering, relative to $2xCO_2$ (Figures S5a and S5b). Exceptions to this response are found in the central U.S., Central America, northern Africa, and southern

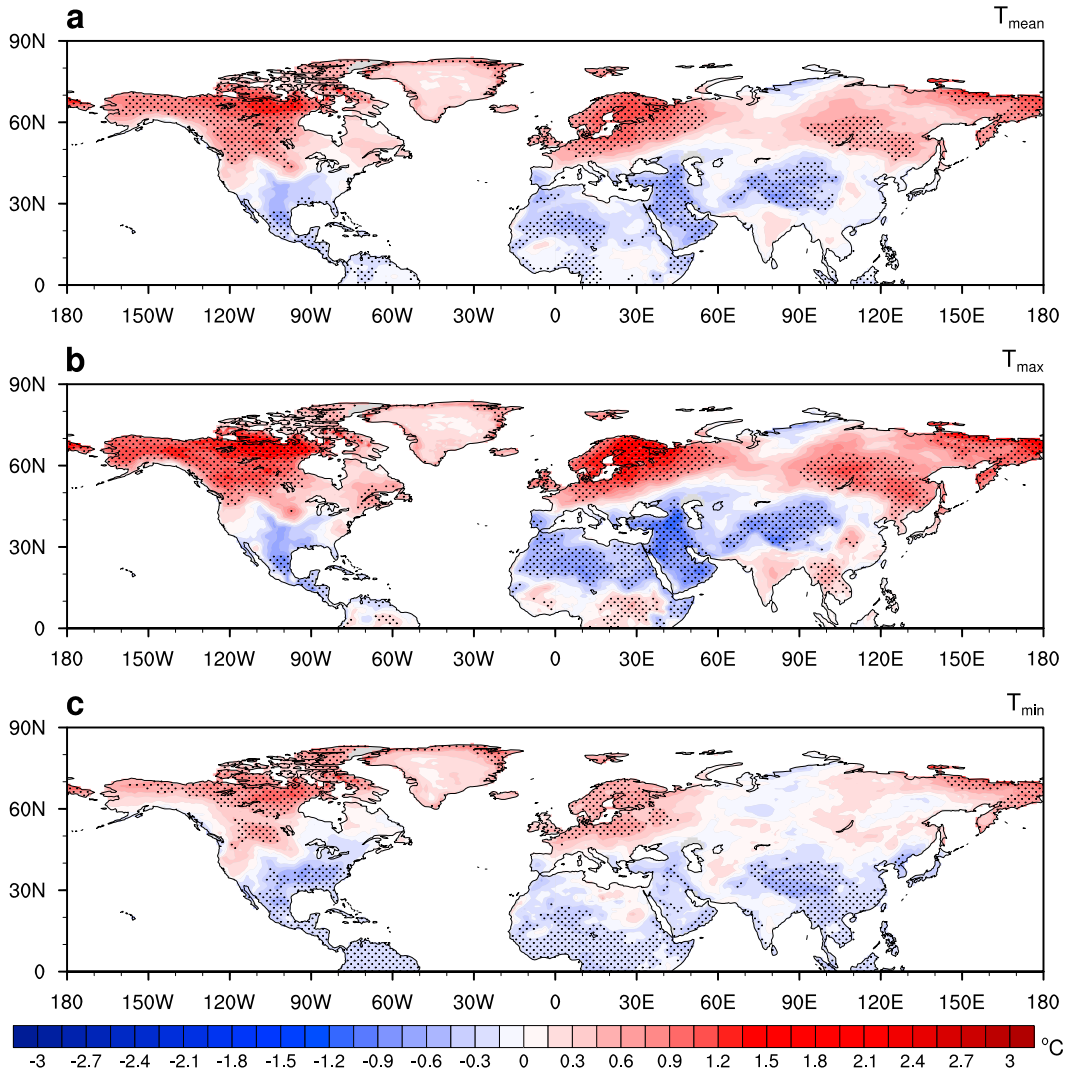

Figure 1. June–August mean land surface air temperature changes (°C) for the ensemble mean of the SolarGeo simulations, relative to the ensemble mean of the Control simulations. Stippling indicates statistically significant changes at the 95% confidence level. (a) Mean daily temperature (T_{mean}). (b) Maximum daily temperature (T_{max}). (c) Minimum daily temperature (T_{min}).

Europe where both precipitation and ET increase. As a result changes in P-ET are spatially variable, with large areas of increase over North America and Asia and areas of decrease in China, India, and Southeast Asia (Figure S5c). Soil moisture mostly increases, as the decrease in ET reduces the tendency of the soils to dry out with greenhouse warming (Figure S5d).

3.2. Regional Distributions

To further investigate changes in regional climate variability, a set of histograms showing the distributions of JJA mean T_{max} averaged over six regions is shown in Figure S6. The regions represent major continental interior climate zones in the Northern Hemisphere, and all encompass an area of 10° in latitude and 15° in longitude, with the exception of the Sahel which is defined by a smaller latitude band of 6° due to the size of the semiarid land area. Under solar geoengineering relative to present day, there is a positive shift in the mean of the T_{max} distributions observed in all regions except the central U.S., where there is very little change in T_{max}, and the Sahel, where T_{max} decreases. We also calculate changes in standard deviation and skewness to examine effects on higher-order moments of the T_{max} distributions. The central U.S., western Europe, and western Russia show a decrease in standard deviation, while Siberia

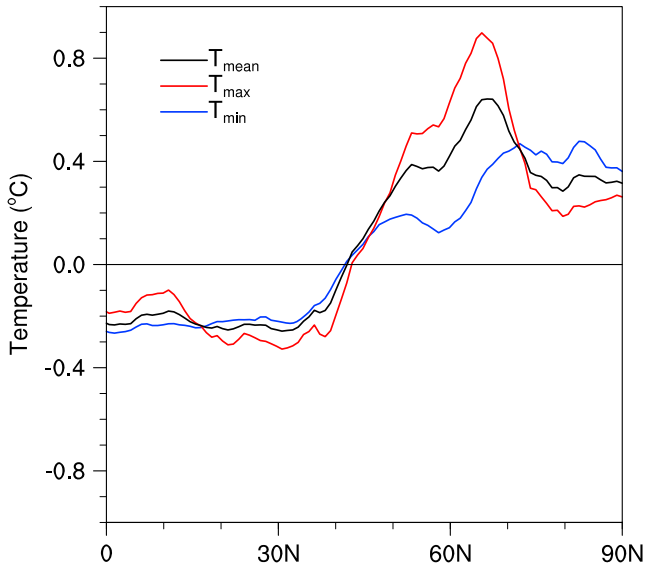

Figure 2. Zonal mean, June–August mean surface air temperature changes (°C) for the ensemble mean of the SolarGeo simulations, relative to the ensemble mean of the Control simulations. The zonal mean is calculated over all grid points (land and ocean) to better show changes in the pole-to-equator temperature gradient. Mean temperature (T_{mean}) in black, maximum temperature (T_{max}) in red, and minimum temperature (T_{min}) in blue.

and India show an increase. The change in variance in the Sahel is very small. Distribution skewness decreases in all regions under solar geoengineering, except in western Russia and the Sahel.

A similar set of histograms for JJA total precipitation is shown in Figure S7. Instead of a regional average, precipitation distributions are taken from a single grid point that represents the approximate midpoint of each region. The distribution mean decreases in all regions except the Sahel. Furthermore the distribution standard deviation decreases in all regions except Siberia and the Sahel, where anomalously wet and dry summers are observed under solar geoengineering and act to increase distribution variance. Distribution skewness increases in all the regions except for western Europe and the central U.S.

3.3. Extreme Temperature and Precipitation Events

A summary of how heat wave events change under solar geoengineering is shown in Table 1. Five different durations are selected to explore the range of event lengths. For each region, the minimum T_{max} threshold is chosen based on the Control ensemble JJA mean T_{max} plus one standard deviation, allowing the regional definition of a heat wave to vary and sample the high end of the local temperature distribution. For each duration and threshold within a given region, the time series of JJA daily T_{max} is analyzed for consecutive days above the specified temperature threshold. The number of events is summed across each summer and then summed across ensemble members to generate an ensemble total number of heat wave events. Though the frequency of events in a control climate will vary within each region, looking at the changes across many durations and region-specific thresholds gives a better sense of how extremes are changing locally. In western Russia and Siberia, solar geoengineering generally increases heat wave events relative to present day (Figures 4 and 5). In the central U.S. and the Sahel, solar geoengineering decreases heat wave events (Figures 6 and 7). Western Europe shows some increase in heat waves, but with less consistency across durations and temperature thresholds (Figure S8 and Table 1). This region is likely sensitive to the chosen spatial area, as evident from Figure 1b. In India, solar geoengineering decreases some heat wave events, while high threshold events increase (Figure S9 and Table 1).

A summary of how consecutive dry day events change under solar geoengineering, relative to the Control simulations, is shown in Table 2. Six different durations are chosen to explore a range of event lengths. As with the precipitation distributions, data are taken from a single grid point rather than a regional average. A dry day is defined as a day when total rainfall is less than 1 mm. Consecutive dry days are then analyzed from the time series of daily JJA precipitation for each regional point. As with heat wave events, the number of dry day events is summed across each summer and then summed across ensemble members. Relative to present day, solar geoengineering mostly increases the number of short duration (≤7 day) events for all regions except western Russia and the Sahel, while it mostly decreases the number of long duration (≥10 day) events in those regions.

Heat wave events nearly universally decrease in all regions, and for all durations and temperature thresholds, under solar geoengineering relative to $2xCO_2$ (Table S2). The exception to this result is seen at low durations and temperature thresholds in some regions, where heat waves are so common in the $2xCO_2$ ensemble that low threshold events blend together and not as many unique events are counted. This also explains why some of the low threshold 10 day events in the $2xCO_2$ panels in Figures 4–6 show a drop in event frequency relative to the middle threshold events. In India and western Russia the number of dry day events increases under solar geoengineering relative to $2xCO_2$ (Table S3). Other regions show a mix of increases and decreases at different event durations, though most show increases in short duration events. However, in the Sahel periods of low precipitation decrease in frequency at all durations.

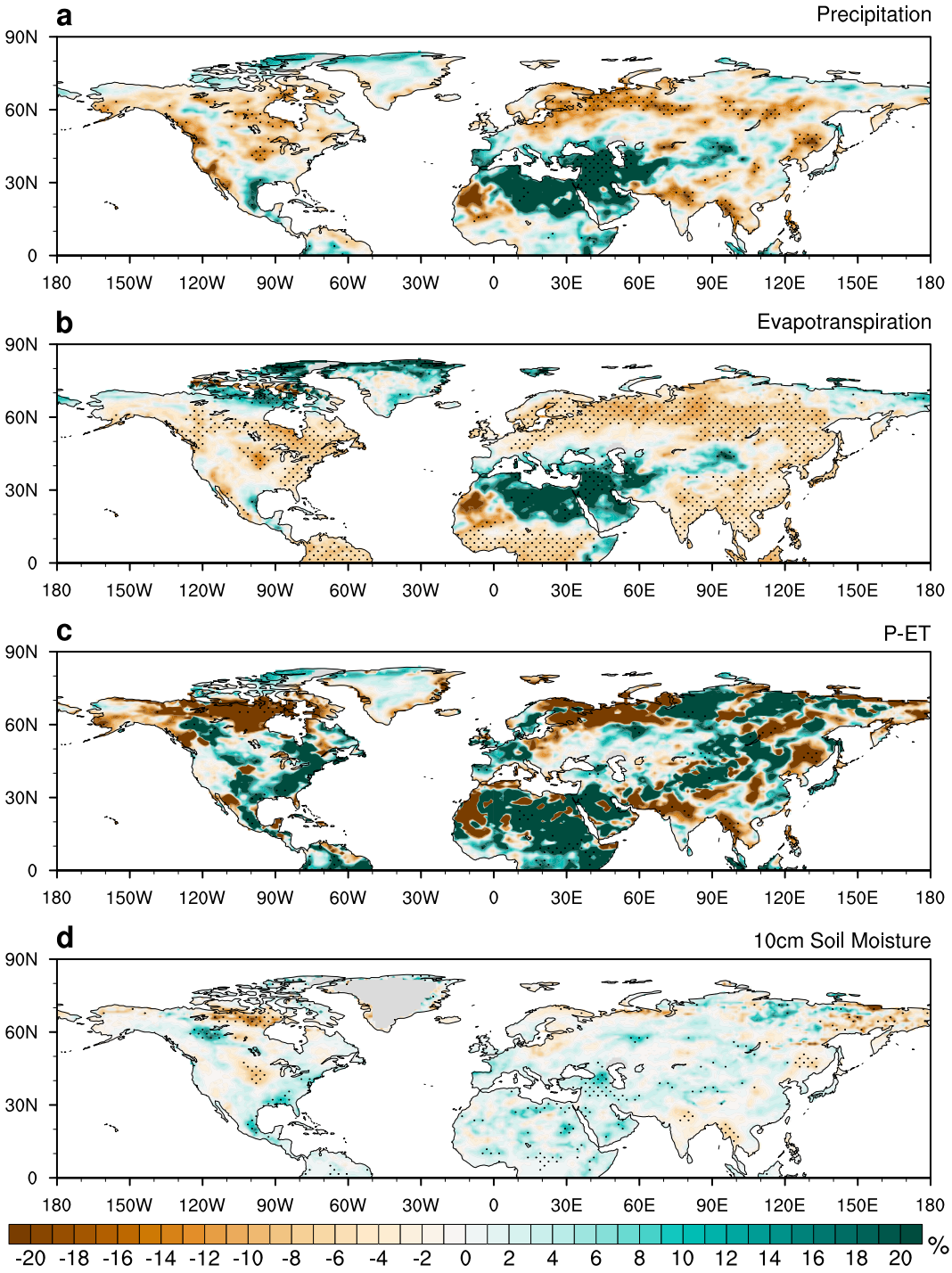

Figure 3. June–August mean land surface water changes (%) for the ensemble mean of the SolarGeo simulations, relative to the ensemble mean of the Control simulations. Stippling indicates statistically significant changes at the 95% confidence level. (a) Precipitation. (b) Evapotranspiration. (c) Precipitation minus evapotranspiration (P-ET). (d) Soil moisture of the top 10 cm.

4. Discussion

4.1. Model Variability in the Context of Historical Observations

To place the modeled climate variability in the context of observations, we compare the resulting temperature and precipitation extremes in the central U.S. with historical data. For this comparison we utilize the

Table 1
Change in the Number of Regional Heat Wave Events for the SolarGeo Ensemble, Relative to the Control Ensemble

Event Length (Days)	T_{max} Threshold				
Central U.S. (35–45°N, 105–90°W)	≥ 43°C	≥41°C	≥39°C	≥37°C	≥35°C
3	1	−4	−5	−10	−4
5	−1	1	1	−13	−10
7	0	2	1	−14	−3
10	0	1	1	−4	−5
14	0	0	0	−2	−7
Siberia (60–70°N, 90–105°E)	≥28°C	≥26°C	≥24°C	≥22°C	≥20°C
3	4	12	−2	15	20
5	4	9	3	−2	9
7	2	3	0	−5	7
10	2	2	0	4	6
14	0	1	1	−1	−2
Western Europe (40–50°N, 0–15°E)	≥36°C	≥34°C	≥32°C	≥30°C	≥28°C
3	0	−13	−9	4	7
5	0	−2	−4	1	12
7	0	0	0	−7	9
10	0	0	−2	−2	−1
14	0	0	0	4	1
India (20–30°N, 70–85°E)	≥44°C	≥42°C	≥40°C	≥38°C	≥36°C
3	−1	−1	−2	3	−5
5	0	0	−2	1	−7
7	0	2	2	−1	−3
10	0	2	4	−1	2
14	0	−1	6	2	5
Western Russia (50–60°N, 35–50°E)	≥37°C	≥35°C	≥33°C	≥31°C	≥29°C
3	0	8	−3	6	2
5	0	6	6	0	3
7	1	1	8	−1	−8
10	0	1	5	0	3
14	0	1	0	−2	0
Sahel (14–20°N, 5–20°E)	≥43°C	≥42°C	≥41°C	≥40°C	≥39°C
3	−4	−3	−15	−15	−7
5	0	−1	−5	−18	−16
7	0	−2	−4	−8	−13
10	0	0	−2	−7	−6
14	0	0	−1	−3	−6

Note. A heat wave is defined as a certain number of consecutive days where the regional average June–August daily maximum temperature (T_{max}) is greater than or equal to a threshold value.

Global Historical Climatology Network-Daily (GHCND) database (Menne et al., 2012). This network includes observations of more than 40 meteorological variables at over 75,000 stations worldwide, including daily maximum temperature and precipitation. We calculate the number of heat wave and dry day events across 31 summers (1982–2012) over the same central U.S. region used in the modeling results. Ten day heat waves are much less frequent in the observations than the model control ensemble (Figure S10), though the number of low precipitation events is comparable across different event durations (Figure S11). The lack of heat wave events in the observations is likely due to the positive bias in model surface temperatures, which is in part attributed to the slab ocean model forcing (Bitz et al., 2012; Dagon & Schrag, 2016). This result gives us some context for the range of regional variability captured by the model ensemble members as compared with historical observations. We can then more closely examine the shift in modeled variability under solar geoengineering and explore the mechanisms related to that response.

4.2. Large-Scale Features in the Northern Hemisphere Response

The spatial variability of changes in boreal summer surface temperature under uniform solar geoengineering shows a strong meridional pattern where low latitudes cool and high latitudes warm, relative to a control climate (Figure 1). This pattern is primarily driven by the spatial variation of insolation, which is larger in

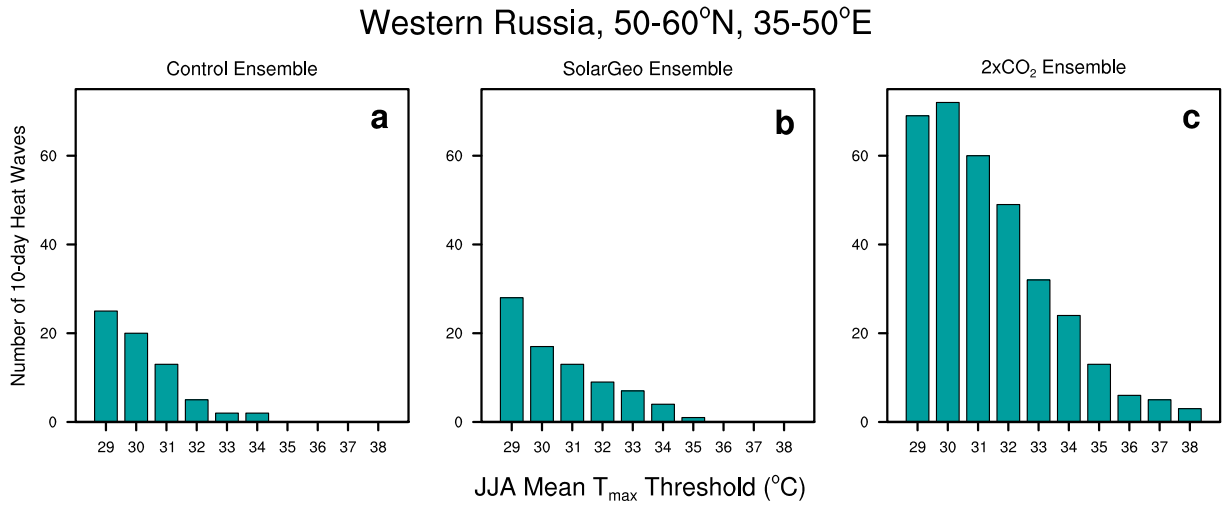

Figure 4. Total number of 10 day heat wave events for each ensemble in western Russia, where heat waves are defined by consecutive days greater than or equal to regional average June–August (JJA) daily maximum surface temperature (T_{max}) thresholds (°C). (a) Control ensemble. (b) SolarGeo ensemble. (c) 2xCO_2 ensemble.

the tropics than at the poles. This result demonstrates the limitation of globally uniform changes in incoming solar radiation to counteract temperature increases from well-mixed greenhouse gases, as shown in previous studies (e.g., Kravitz, Caldeira, et al., 2013). Spatially varying changes in solar radiation could act to diminish these issues. A few recent studies that do use spatiotemporal tailoring of solar geoengineering find that it is more effective at minimizing zonal mean climate changes (e.g., Kravitz et al., 2016; MacMartin et al., 2013), though models cannot simultaneously stabilize global temperature and precipitation anomalies (Ricke et al., 2010).

Land surface hydrology does not show a similar spatial pattern in the response to uniform solar geoengineering. There is a weak meridional gradient in summertime precipitation (Figure 3a) and evapotranspiration (Figure 3b) over the European and Asian continents, where these quantities decrease in high latitudes and partially increase in low latitudes. However a north-south gradient is not evident in the hydrologic response over North America. The lack of a meridional pattern is also shown in the regionally heterogeneous responses of P-ET (Figure 3c) and soil moisture (Figure 3d). A decrease in the pole-to-equator temperature gradient that is evident under uniform solar geoengineering (Figure 2) is likely to alter atmospheric circulation, which could further influence land surface hydrology through convective and large-scale precipitation changes. These

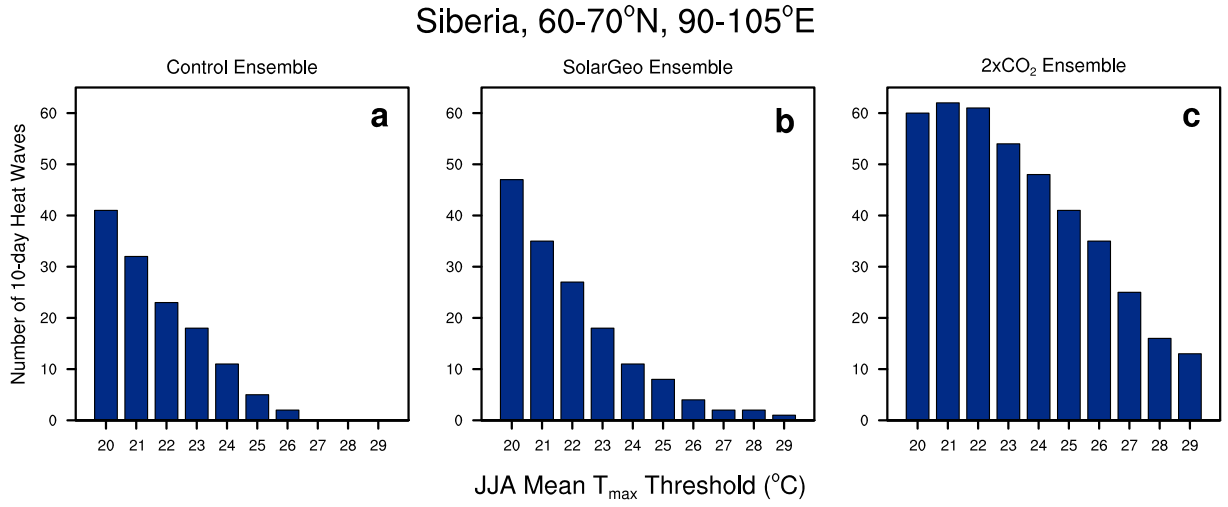

Figure 5. As in Figure 4, for Siberia.

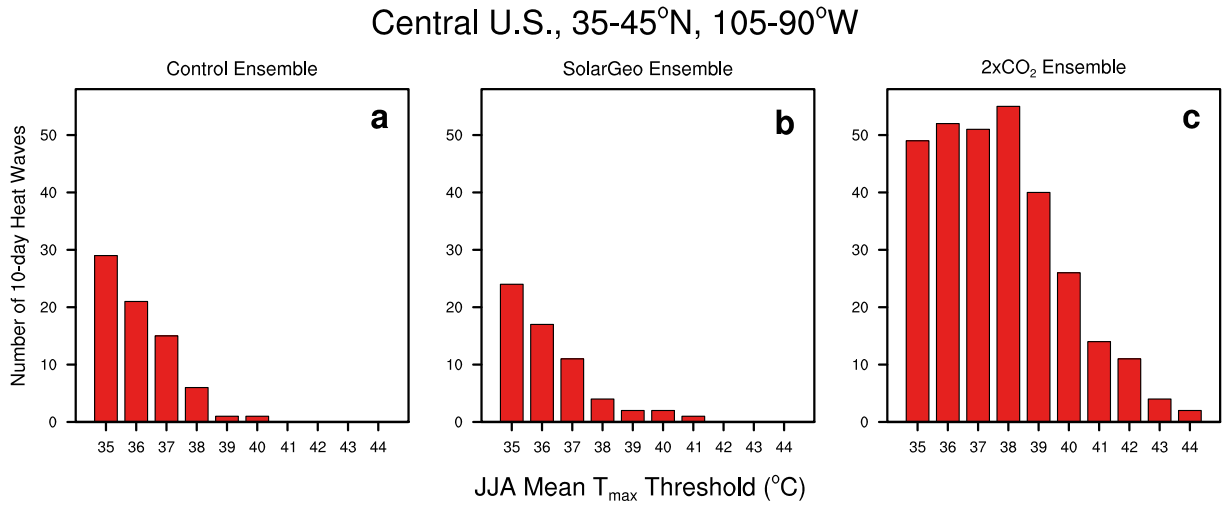

Figure 6. As in Figure 4, for the central U.S.

results indicate that a spatially varying solar geoengineering scheme may not completely compensate for changes in land surface hydrology (Ban-Weiss & Caldeira, 2010), though efforts to reduce changes in the pole-to-equator temperature gradient could have positive effects.

Regional changes in summertime maximum temperature from uniform solar geoengineering relative to present day have potential benefits for human health and agriculture in places where there is cooling of summer heat extremes, for example, the central U.S., northern Africa, the Middle East, and central Asia (Figure 1b). There are potential negative impacts to an increase of summer heat extremes in high northern latitudes during boreal summer, again when solar geoengineering is compared to present day. Both of these results echo the response of maximum daily temperature in the study by Curry et al. (2014). Changes in summertime precipitation (Figure 3a), ET (Figure 3b), and soil moisture (Figure 3d) are spatially heterogeneous and thus have varying consequences for agriculture and vegetation (Tilmes et al., 2013). The decrease in boreal summer ET under solar geoengineering relative to the control climate is driven on a global scale by a lack of solar radiation to supply surface energy, as demonstrated by the comparison with a high-CO_2 world (Figure S5b).

4.3. Changes in Regional Temperature and Precipitation Variability

To explore shifts in variance related to extreme weather events, we focus on daily temperature and precipitation thresholds to explore a variety of event durations and magnitudes and quantify events in terms of their

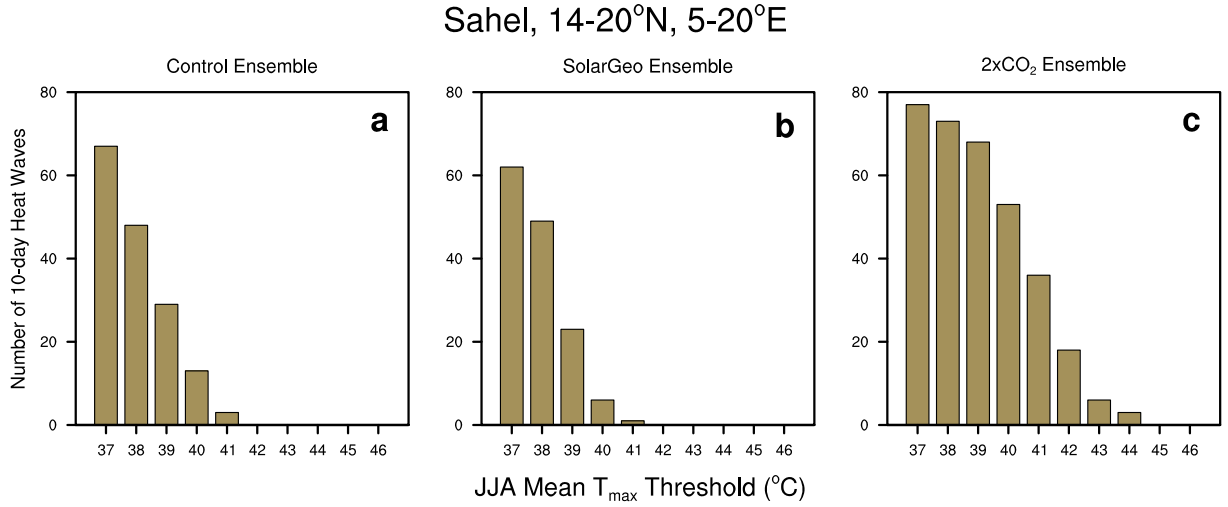

Figure 7. As in Figure 4, for the Sahel.

Table 2
Change in the Number of Regional June–August Dry Day Events for the SolarGeo Ensemble, Relative to the Control Ensemble

	3 days <1 mm	5 days	7 days	10 days	14 days	21 days
Central U.S., 40°N, 97°W	−4	9	4	−1	−1	0
Siberia, 65°N, 98°E	14	3	−3	−2	−1	0
W. Europe, 45°N, 8°E	2	−4	8	0	−1	0
India, 25°N, 78°E	14	8	6	−1	1	−2
W. Russia, 55°N, 43°E	−5	−5	6	4	3	0
Sahel, 17°N, 13°E	−2	−2	−3	6	−5	2

Note. A dry day event is defined as a certain number of consecutive days where daily total precipitation is less than 1 mm.

frequency. Rather than attempt to define drought on a seasonal scale, we examine changes in consecutive dry days based on daily total precipitation. Gaps in precipitation can contribute to drought but there are other factors such as snowpack level, soil moisture, evapotranspiration, and runoff that play an important role. Our results also utilize different spatial areas to analyze extreme events. Temperature events such as heat waves can be more easily averaged over a larger spatial domain. Hydrology is more variable and thus we focus on a single grid point rather than an entire region.

At a regional scale we see two patterns in the variability response to solar geoengineering with coherent mechanisms that we can identify in the model simulations. The first is characterized by increases in extreme

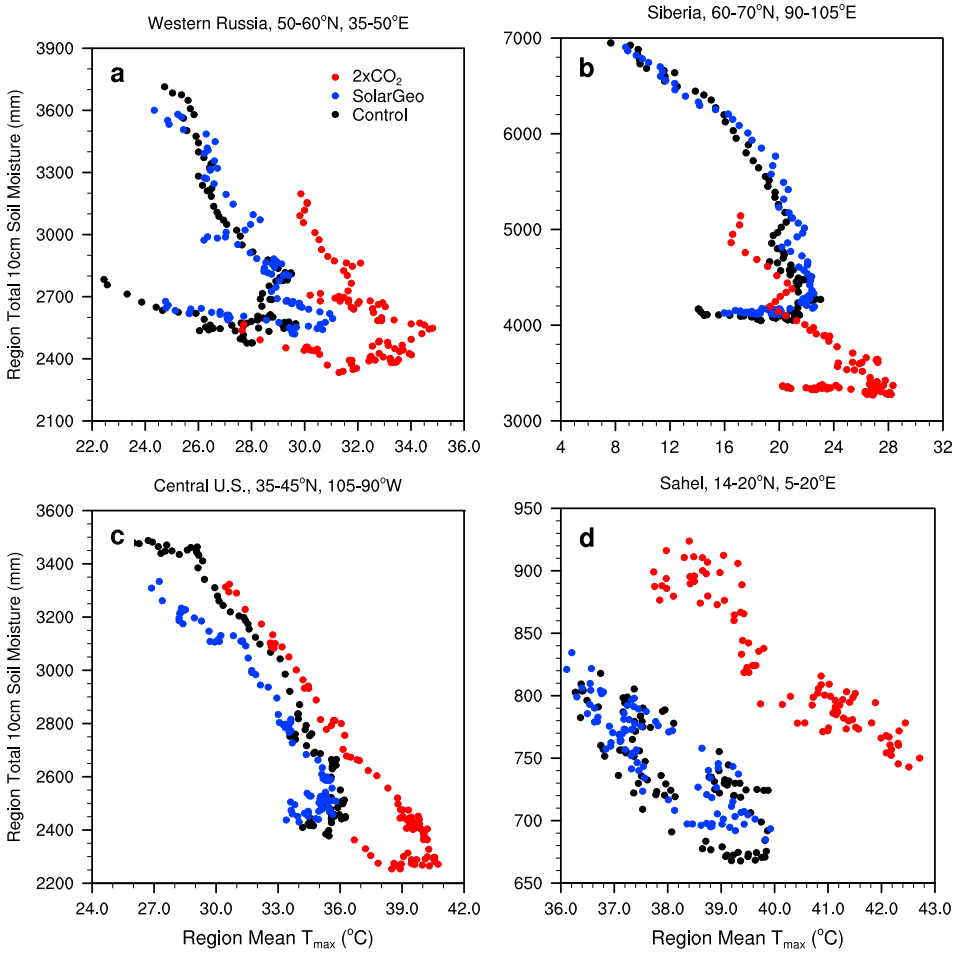

Figure 8. June–August daily scatterplot of region total soil moisture of the top 10 cm (mm) versus region mean maximum temperature (T_{max}) (°C) shown in black for the ensemble mean of the Control simulations, blue for the ensemble mean of the SolarGeo simulations, and red for the ensemble mean of the $2xCO_2$ simulations. (a) Western Russia (b) Siberia. (c) Central U.S. (d) Sahel.

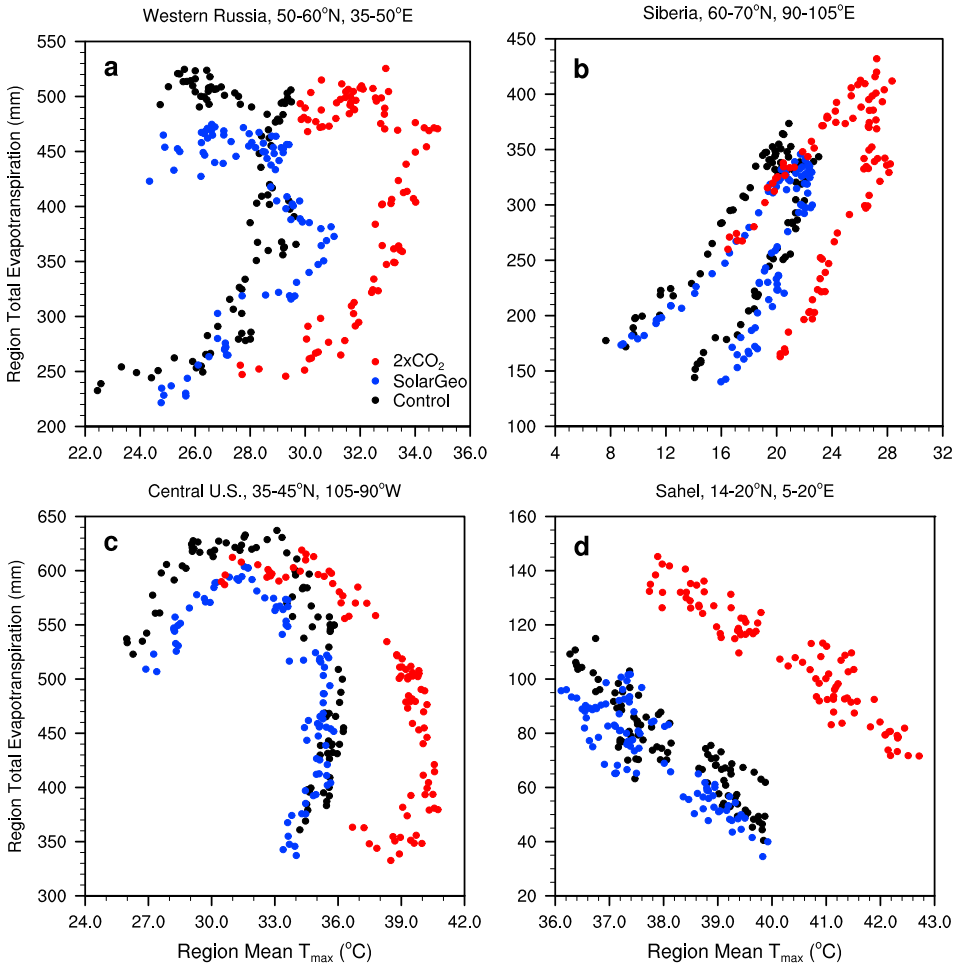

Figure 9. As in Figure 8, for region total evapotranspiration (mm) versus region mean maximum temperature (T_{max}) (°C).

temperature and decreases in precipitation under solar geoengineering relative to a present day control climate, as evident in western Russia and Siberia. In particular, heat waves tend to increase in frequency in both regions under solar geoengineering (Figures 4 and 5). The mechanistic reason for this outcome is that the coupling of surface soil moisture and air temperature drives maximum temperatures to increase (Figures 8a and 8b). Soils dry out over the course of the summer as T_{max} increases, and this relationship is strengthened under solar geoengineering. The drop in soil moisture is likely related to changes in evapotranspiration, which increases during the highest temperature days (Figures 9a and 9b). This observation points to both increased evaporation driving soil moisture to decline and the importance of the physiological effects of decreased solar radiation and increased CO_2 on plant water cycling.

The second regional pattern is characterized by decreases in extreme temperature, as evident in the central U.S. and the Sahel. Both regions show a decrease in the number of heat wave events under solar geoengineering, with the Sahel showing a robust decrease in event frequency (Table 1 and Figures 6 and 7). This result is due to wetter soils (Figures 8c and 8d), caused by a decrease in total summer ET (Figures 9c and 9d). In the central U.S., ET decreases due to the change in atmospheric CO_2 concentration and the associated decreases in stomatal conductance and transpiration. In the Sahel, the change in ET is driven by the decrease in solar radiation rather than CO_2 forcing (Figure S5). The Sahel also shows a decrease in dry day events and is the region that shows the most consistent response across different event durations (Table 2).

We include the 2xCO_2 ensemble to provide an additional comparison climate for the solar geoengineering ensembles. Both a comparison to present day and greenhouse climates are interesting and valid assessments to make for solar geoengineering, though they provide different information. The contrast between them

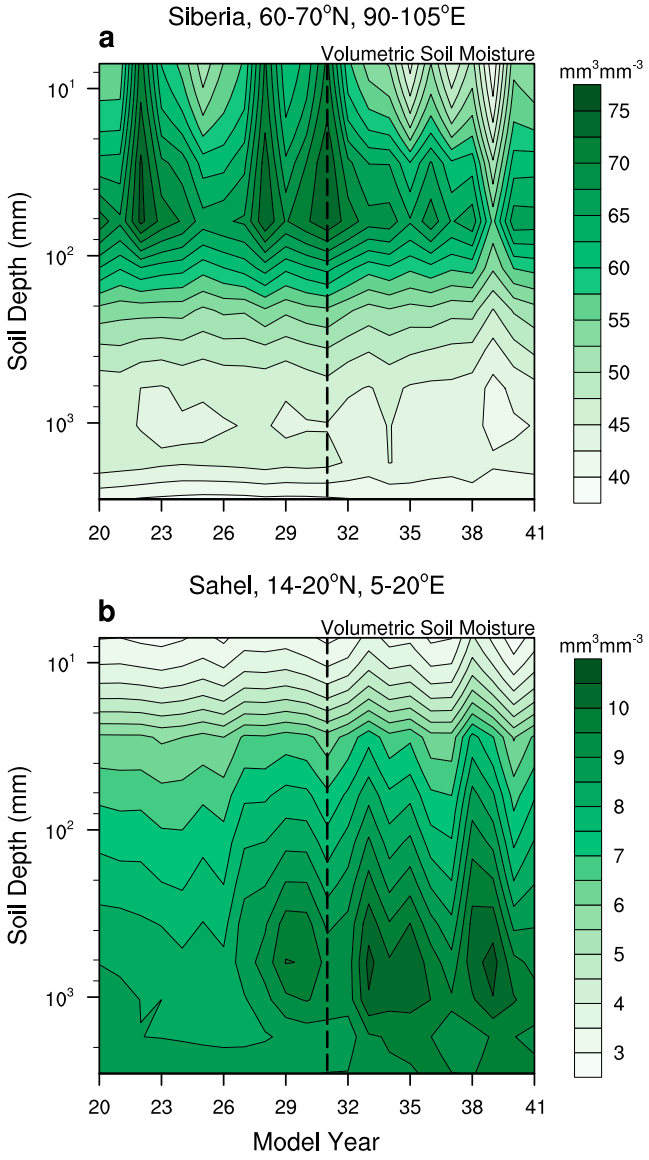

Figure 10. Evolution of annual mean region total volumetric soil moisture ($mm^3\ mm^{-3}$) with depth, for the last 10 years of the model control spin-up and for 10 years after solar geoengineering is imposed (shown by a vertical dashed line in year 31). (a) Siberia. (b) Sahel.

offers a way to explore what changes are driving specific impacts (e.g., the direct effect of CO_2 on vegetation or the radiative effect of a greenhouse gas on surface climate). Extreme high temperatures uniformly decrease under solar geoengineering relative to a doubled CO_2 climate (Figure S4), and as a result, the frequency of heat wave events largely decreases across all regions, event durations, and temperature thresholds (Table S2). On average total summertime precipitation decreases, though in the central U.S. and western Europe precipitation and ET both increase (Figure S5). The increased water cycling in these regions leads to a decrease in the frequency of consecutive dry days, except for some short duration events (Table S3). The Sahel also shows a robust decrease in dry day events under solar geoengineering relative to $2xCO_2$, though in other regions dry day events increase in frequency.

4.4. Robustness of the Model Response to Solar Geoengineering

The interannual variability in the model could overpower the regional changes under solar geoengineering relative to present day. To test the robustness of our results to changing initial conditions, we explore the timescale of the regional climate response to solar geoengineering. The SolarGeo ensemble members start after an additional 10 years of simulation spin-up time with solar geoengineering conditions, and there could be changes in climate during these intervening years that would impact the variability results. Indeed, we find that Siberia and the Sahel show trends in the hydrologic response during the model adjustment to solar geoengineering, indicating that especially in these places the timescale matters. While soil moisture in those regions does not respond immediately to solar geoengineering, during the subsequent model years the soil column dries out as soil evaporation increases in Siberia (Figure 10a) and gets wetter as precipitation increases in the Sahel (Figure 10b). This result shows that although the modeled variability response to solar geoengineering is initially of smaller magnitude, the response strengthens and becomes robust after letting the model adjust to the external forcing of increased CO_2 and decreased solar radiation.

Though we include additional spin-up time for the model to adjust to solar geoengineering, the longest timescales we capture are 10–40 years. It is expected that solar geoengineering will impact the land-sea temperature contrast and have other feedbacks on global atmospheric circulation that may take multiple decades to be realized (Ferraro et al., 2014; Irvine et al., 2016; McCusker et al., 2012; Niemeier et al., 2013). In constructing our ensembles we aim to capture close to stationary distributions from which we compare the resulting statistics. Our results show that changes in variability are evident under solar geoengineering in our idealized model setup. Further testing using a variety of models and implementation techniques is required to fully understand mechanisms that cause regional variability to change under solar geoengineering.

5. Conclusions

Solar geoengineering modeled as uniform changes in incoming solar radiation has demonstrated the ability to counteract CO_2-driven increases in surface temperature, but regional anomalies persist in temperature extremes and the hydrologic cycle. Here we find that using a uniform decrease in the solar constant to mitigate global mean temperature changes exhibits a strong meridional gradient in Northern Hemisphere summer surface temperature, with residual cooling in low latitudes and warming in high latitudes. This gradient is stronger in maximum daily temperature than the gradient in minimum daily temperature, with implications for atmospheric circulation and hydrology through changes in the pole-to-equator

temperature gradient that could affect the Hadley circulation and poleward heat transport. Summer precipitation does not show a similarly strong north-south gradient, and it remains unclear whether land surface hydrology will be as responsive to spatially tailored solar geoengineering schemes, where decreases in solar radiation remain constant with longitude but vary with latitude.

Using an ensemble approach, we show that in almost every region, heat waves and consecutive dry days decrease in frequency in a world with solar geoengineering relative to a doubled CO_2 climate. However, our results show that this method is not without consequences, and some regional extreme events increase under solar geoengineering relative to present day. For example, the drying in western Russia and Siberia is connected with the increase in heat wave occurrence in those regions through evapotranspiration and soil moisture feedbacks. Regions such as the central U.S. and the Sahel show decreases in extreme heat along with increased surface water storage. While the large-scale global responses are observed in the model immediately after solar geoengineering is imposed, we identify trends in modeled soil moisture in Siberia and the Sahel that impact the regional response after a period of 5–10 years. Given the likelihood of an increasing number of extreme events with future climate change, these results underline important tradeoffs between solar geoengineering and unmitigated global warming. Finally, these results were found in a single model with an idealized solar reduction, and it will be crucial to test the outcomes across many different climate models, including when solar geoengineering is simulated explicitly (e.g., using stratospheric aerosols).

Acknowledgments

The computations in this paper were run on the Odyssey cluster supported by the FAS Division of Science, Research Computing Group at Harvard University. We thank Zhiming Kuang for the use of his computational resources. We thank the Editor and three anonymous reviewers for suggestions that improved the paper. The National Center for Atmospheric Research Community Earth System Model (CESM) is available at http://www.cesm.ucar.edu/models/current.html. The Global Historical Climatology Network (GHCN) database is available at https://www.ncdc.noaa.gov/data-access/land-based-station-data/land-based-datasets/global-historical-climatology-network-ghcn. All materials that have contributed to the results, including CESM model output, are available on request. Requests for data should be directed to the corresponding author K. Dagon (kdagon@fas.harvard.edu).

References

Allen, M. R., & Ingram, W. J. (2002). Constraints on future changes in climate and the hydrologic cycle. *Nature*, *419*(6903), 224–232. https://doi.org/10.1038/nature01092

Andrews, T., Forster, P. M., & Gregory, J. M. (2009). A surface energy perspective on climate change. *Journal of Climate*, *22*(10), 2557–2570. https://doi.org/10.1175/2008jcli2759.1

Aswathy, N., Boucher, O., Quaas, M., Niemeier, U., Muri, H., Mulmenstadt, J., & Quaas, J. (2015). Climate extremes in multi-model simulations of stratospheric aerosol and marine cloud brightening climate engineering. *Atmospheric Chemistry and Physics*, *15*(16), 9593–9610. https://doi.org/10.5194/acp-15-9593-2015

Bala, G., Caldeira, K., & Nemani, R. (2010). Fast versus slow response in climate change: Implications for the global hydrological cycle. *Climate Dynamics*, *35*(2-3), 423–434. https://doi.org/10.1007/s00382-009-0583-y

Bala, G., Duffy, P. B., & Taylor, K. E. (2008). Impact of geoengineering schemes on the global hydrological cycle. *Proceedings of the National Academy of Sciences of the United States of America*, *105*(22), 7664–7669. https://doi.org/10.1073/pnas.0711648105

Ban-Weiss, G. A., & Caldeira, K. (2010). Geoengineering as an optimization problem. *Environmental Research Letters*, *5*(3). https://doi.org/10.1088/1748-9326/5/3/034009

Barnett, D. N., Brown, S. J., Murphy, J. M., Sexton, D. M. H., & Webb, M. J. (2006). Quantifying uncertainty in changes in extreme event frequency in response to doubled CO_2 using a large ensemble of GCM simulations. *Climate Dynamics*, *26*(5), 489–511. https://doi.org/10.1007/s00382-005-0097-1

Berg, A., Findell, K., Lintner, B., Giannini, A., Seneviratne, S. I., van den Hurk, B., … Milly, P. C. D. (2016). Land-atmosphere feedbacks amplify aridity increase over land under global warming. *Nature Climate Change*, *6*(9), 869–874. https://doi.org/10.1038/Nclimate3029

Betts, R. A., Boucher, O., Collins, M., Cox, P. M., Falloon, P. D., Gedney, N., … Webb, M. J. (2007). Projected increase in continental runoff due to plant responses to increasing carbon dioxide. *Nature*, *448*(7157), 1037–1041. https://doi.org/10.1038/nature06045

Bi, H. Y., Ma, J. W., Zheng, W. J., & Zeng, J. Y. (2016). Comparison of soil moisture in GLDAS model simulations and in situ observations over the Tibetan Plateau. *Journal of Geophysical Research: Atmospheres*, *121*, 2658–2678. https://doi.org/10.1002/2015JD024131

Bitz, C. M., Shell, K. M., Gent, P. R., Bailey, D. A., Danabasoglu, G., Armour, K. C., … Kiehl, J. T. (2012). Climate sensitivity of the Community Climate System Model, version 4. *Journal of Climate*, *25*(9), 3053–3070. https://doi.org/10.1175/Jcli-D-11-00290.1

Bonan, G. B., Levis, S., Kergoat, L., & Oleson, K. W. (2002). Landscapes as patches of plant functional types: An integrating concept for climate and ecosystem models. *Global Biogeochemical Cycles*, *16*(2), 5-1–5-23. https://doi.org/10.1029/2000GB001360

Caldeira, K., & Wood, L. (2008). Global and Arctic climate engineering: Numerical model studies. *Philosophical Transactions of the Royal Society A: Mathematical, Physical and Engineering Sciences*, *366*(1882), 4039–4056. https://doi.org/10.1098/rsta.2008.0132

Cao, L., Bala, G., & Caldeira, K. (2012). Climate response to changes in atmospheric carbon dioxide and solar irradiance on the time scale of days to weeks. *Environmental Research Letters*, *7*(3). https://doi.org/10.1088/1748-9326/7/3/034015

Clark, R. T., Brown, S. J., & Murphy, J. M. (2006). Modeling northern hemisphere summer heat extreme changes and their uncertainties using a physics ensemble of climate sensitivity experiments. *Journal of Climate*, *19*(17), 4418–4435. https://doi.org/10.1175/Jcli3877.1

Cohen, J., Screen, J. A., Furtado, J. C., Barlow, M., Whittleston, D., Coumou, D., … Jones, J. (2014). Recent Arctic amplification and extreme mid-latitude weather. *Nature Geoscience*, *7*(9), 627–637. https://doi.org/10.1038/Ngeo2234

Crutzen, P. J. (2006). Albedo enhancement by stratospheric sulfur injections: A contribution to resolve a policy dilemma? *Climatic Change*, *77*(3-4), 211–220. https://doi.org/10.1007/s10584-006-9101-y

Curry, C. L., Sillmann, J., Bronaugh, D., Alterskjaer, K., Cole, J. N. S., Ji, D., … Yang, S. (2014). A multimodel examination of climate extremes in an idealized geoengineering experiment. *Journal of Geophysical Research: Atmospheres*, *119*, 3900–3923. https://doi.org/10.1002/2013JD020648

Dagon, K., & Schrag, D. P. (2016). Exploring the effects of solar radiation management on water cycling in a coupled land-atmosphere model. *Journal of Climate*, *29*(7), 2635–2650. https://doi.org/10.1175/Jcli-D-15-0472.1

Deser, C., Phillips, A., Bourdette, V., & Teng, H. Y. (2012). Uncertainty in climate change projections: The role of internal variability. *Climate Dynamics*, *38*(3-4), 527–546. https://doi.org/10.1007/s00382-010-0977-x

Doutriaux-Boucher, M., Webb, M. J., Gregory, J. M., & Boucher, O. (2009). Carbon dioxide induced stomatal closure increases radiative forcing via a rapid reduction in low cloud. *Geophysical Research Letters*, *36*, L02703. https://doi.org/10.1029/2008GL036273

Emanuel, K., Ravela, S., Vivant, E., & Risi, C. (2006). A statistical deterministic approach to hurricane risk assessment. *Bulletin of the American Meteorological Society*, *87*(3), 299–314. https://doi.org/10.1175/Bams-87-3-299

Ferraro, A. J., Highwood, E. J., & Charlton-Perez, A. J. (2014). Weakened tropical circulation and reduced precipitation in response to geoengineering. *Environmental Research Letters*, *9*(1). https://doi.org/10.1088/1748-9326/9/1/014001

Field, C. B., Jackson, R. B., & Mooney, H. A. (1995). Stomatal responses to increased CO_2: Implications from the plant to the global scale. *Plant, Cell and Environment*, *18*(10), 1214–1225. https://doi.org/10.1111/j.1365-3040.1995.tb00630.x

Fischer, E. M., Beyerle, U., & Knutti, R. (2013). Robust spatially aggregated projections of climate extremes. *Nature Climate Change*, *3*(12), 1033–1038. https://doi.org/10.1038/Nclimate2051

Fischer, E. M., Rajczak, J., & Schar, C. (2012). Changes in European summer temperature variability revisited. *Geophysical Research Letters*, *39*, L19702. https://doi.org/10.1029/2012GL052730

Fischer, E. M., Seneviratne, S. I., Luthi, D., & Schar, C. (2007). Contribution of land-atmosphere coupling to recent European summer heat waves. *Geophysical Research Letters*, *34*, L06707. https://doi.org/10.1029/2006GL029068

Franks, P. J., Adams, M. A., Amthor, J. S., Barbour, M. M., Berry, J. A., Ellsworth, D. S., … von Caemmerer, S. (2013). Sensitivity of plants to changing atmospheric CO_2 concentration: From the geological past to the next century. *The New Phytologist*, *197*(4), 1077–1094. https://doi.org/10.1111/nph.12104

Gillett, N. P., Weaver, A. J., Zwiers, F. W., & Wehner, M. F. (2004). Detection of volcanic influence on global precipitation. *Geophysical Research Letters*, *31*, L12217. https://doi.org/10.1029/2004GL020044

Hirschi, M., Seneviratne, S. I., Alexandrov, V., Boberg, F., Boroneant, C., Christensen, O. B., … Stepanek, P. (2011). Observational evidence for soil-moisture impact on hot extremes in southeastern Europe. *Nature Geoscience*, *4*(1), 17–21. https://doi.org/10.1038/Ngeo1032

Iles, C. E., Hegerl, G. C., Schurer, A. P., & Zhang, X. B. (2013). The effect of volcanic eruptions on global precipitation. *Journal of Geophysical Research: Atmospheres*, *118*, 8770–8786. https://doi.org/10.1002/jgrd.50678

Intergovernmental Panel on Climate Change (IPCC) (2012). In C. B. Field, et al. (Eds.), *Managing the risks of extreme events and disasters to advance climate change adaptatione. A Special Report of Working Groups I and II of the Intergovernmental Panel on Climate Change* (pp. 582). Cambridge, United Kingdom and New York: Cambridge University Press.

Intergovernmental Panel on Climate Change (IPCC) (2013). In T. F. Stocker, et al. (Eds.). *Climate change 2013: The physical science basis. Contribution of working group I to the fifth assessment report of the Intergovernmental Panel on Climate Change* (p. 1535). Cambridge, United Kingdom and New York: Cambridge United Kingdom Press.

Irvine, P. J., Kravitz, B., Lawrence, M. G., & Muri, H. (2016). An overview of the earth system science of solar geoengineering. *WIREs Climate Change*, *7*(6), 815–833. https://doi.org/10.1002/wcc.423

Kay, J. E., Deser, C., Phillips, A., Mai, A., Hannay, C., Strand, G., … Vertenstein, M. (2015). The Community Earth System Model (CESM) large ensemble project: A community resource for studying climate change in the presence of internal climate variability. *Bulletin of the American Meteorological Society*, *96*(8), 1333–1349. https://doi.org/10.1175/Bams-D-13-00255.1

Keith, D. W., & MacMartin, D. G. (2015). A temporary, moderate and responsive scenario for solar geoengineering. *Nature Climate Change*, *5*(3), 201–206. https://doi.org/10.1038/Nclimate2493

Kleidon, A., & Renner, M. (2013). A simple explanation for the sensitivity of the hydrologic cycle to surface temperature and solar radiation and its implications for global climate change. *Earth System Dynamics*, *4*(2), 455–465. https://doi.org/10.5194/esd-4-455-2013

Kravitz, B., Caldeira, K., Boucher, O., Robock, A., Rasch, P. J., Alterskjær, K., … Yoon, J.-H. (2013). Climate model response from the geoengineering model Intercomparison Project (GeoMIP). *Journal of Geophysical Research: Atmospheres*, *118*, 8320–8332. https://doi.org/10.1002/jgrd.50646

Kravitz, B., Rasch, P. J., Forster, P. M., Andrews, T., Cole, J. N. S., Irvine, P. J., & Yoon, J.-H. (2013). An energetic perspective on hydrological cycle changes in the Geoengineering Model Intercomparison Project. *Journal of Geophysical Research: Atmospheres*, *118*, 13,087–13,102. https://doi.org/10.1002/2013JD020502

Kravitz, B., MacMartin, D. G., Rasch, P. J., & Jarvis, A. J. (2015). A new method of comparing forcing agents in climate models. *Journal of Climate*, *28*(20), 8203–8218. https://doi.org/10.1175/Jcli-D-14-00663.1

Kravitz, B., MacMartin, D. G., Wang, H. L., & Rasch, P. J. (2016). Geoengineering as a design problem. *Earth System Dynamics*, *7*(2), 469–497. https://doi.org/10.5194/esd-7-469-2016

Lammertsma, E. I., de Boer, H. J., Dekker, S. C., Dilcher, D. L., Lotter, A. F., & Wagner-Cremer, F. (2011). Global CO_2 rise leads to reduced maximum stomatal conductance in Florida vegetation. *Proceedings of the National Academy of Sciences of the United States of America*, *108*(10), 4035–4040. https://doi.org/10.1073/pnas.1100371108

Lawrence, D. M., Lawrence, D. M., Oleson, K. W., Flanner, M. G., Thornton, P. E., Swenson, S. C., … Slater, A. G. (2011). Parameterization improvements and functional and structural advances in version 4 of the community land model. *Journal of Advances in Modeling Earth Systems*, *3*, M03001. https://doi.org/10.1029/2011MS000045

Lee, J. E., Lintner, B. R., Neelin, J. D., Jiang, X., Gentine, P., Boyce, C. K., … Worden, J. (2012). Reduction of tropical land region precipitation variability via transpiration. *Geophysical Research Letters*, *39*, L19704. https://doi.org/10.1029/2012GL053417

Li, H. B., Robock, A., & Wild, M. (2007). Evaluation of Intergovernmental Panel on Climate Change Fourth Assessment soil moisture simulations for the second half of the twentieth century. *Journal of Geophysical Research: Atmospheres*, *112*, D0610. https://doi.org/10.1029/2006JD007455

Lorenz, R., Jaeger, E. B., & Seneviratne, S. I. (2010). Persistence of heat waves and its link to soil moisture memory. *Geophysical Research Letters*, *37*, L09703. https://doi.org/10.1029/2010GL042764

MacMartin, D. G., Keith, D. W., Kravitz, B., & Caldeira, K. (2013). Management of trade-offs in geoengineering through optimal choice of non-uniform radiative forcing. *Nature Climate Change*, *3*(4), 365–368. https://doi.org/10.1038/Nclimate1722

Marsh, D. R., Mills, M. J., Kinnison, D. E., Lamarque, J.-F., Calvo, N., & Polvani, L. M. (2013). Climate change from 1850 to 2005 simulated in CESM1(WACCM). *Journal of Climate*, *26*(19), 7372–7391. https://doi.org/10.1175/JCLI-D-12-00558.1

McCusker, K. E., Battisti, D. S., & Bitz, C. M. (2012). The climate response to stratospheric sulfate injections and implications for addressing climate emergencies. *Journal of Climate*, *25*(9), 3096–3116. https://doi.org/10.1175/Jcli-D-11-00183.1

McKinnon, K. A., Rhines, A., Tingley, M. P., & Huybers, P. (2016). Long-lead predictions of eastern United States hot days from Pacific sea surface temperatures. *Nature Geoscience*, *9*(5), 389–394. https://doi.org/10.1038/Ngeo2687

Menne, M. J., Durre, I., Vose, R. S., Gleason, B. E., & Houston, T. G. (2012). An overview of the Global Historical Climatology Network-Daily database. *Journal of Atmospheric and Oceanic Technology*, *29*(7), 897–910. https://doi.org/10.1175/Jtech-D-11-00103.1

Miralles, D. G., Teuling, A. J., van Heerwaarden, C. C., & de Arellano, J. V. G. (2014). Mega-heatwave temperatures due to combined soil desiccation and atmospheric heat accumulation. *Nature Geoscience*, *7*(5), 345–349. https://doi.org/10.1038/Ngeo2141

Mueller, B., & Seneviratne, S. I. (2012). Hot days induced by precipitation deficits at the global scale. *Proceedings of the National Academy of Sciences of the United States of America*, *109*(31), 12,398–12,403. https://doi.org/10.1073/pnas.1204330109

Neale, R. B., Richter, J. H., Conley, A. J., Park, S., Lauritzen, P. H., Gettelman, A., … Lin, S.-J. (2010). Description of the NCAR Community Atmosphere Model (CAM 4.0) (NCAR Tech. Note TN-485+STR, pp. 212).

Niemeier, U., Schmidt, H., Alterskjaer, K., & Kristjansson, J. E. (2013). Solar irradiance reduction via climate engineering: Impact of different techniques on the energy balance and the hydrological cycle. *Journal of Geophysical Research: Atmospheres*, *118*, 11,905–11,917. https://doi.org/10.1002/2013JD020445

O'Gorman, P. A., Allan, R. P., Byrne, M. P., & Previdi, M. (2012). Energetic constraints on precipitation under climate change. *Surveys in Geophysics*, *33*(3-4), 585–608. https://doi.org/10.1007/s10712-011-9159-6

Oleson, K. W., Lawrence, D., Bonan, G., & Yang, Z. (2013). Technical description of version 4.5 of the Community Land Model (CLM) (NCAR Tech. Note TN-503+STR, 420 pp.). https://doi.org/10.5065/D6RR1W7M

Rasch, P. J., Crutzen, P. J., & Coleman, D. B. (2008). Exploring the geoengineering of climate using stratospheric sulfate aerosols: The role of particle size. *Geophysical Research Letters*, *35*, L02809. https://doi.org/10.1029/2007GL032179

Ricke, K. L., Morgan, G., & Allen, M. R. (2010). Regional climate response to solar-radiation management. *Nature Geoscience*, *3*(8), 537–541. https://doi.org/10.1038/ngeo915

Sellers, P. J., Bounoua, L., Collatz, G. J., Randall, D. A., Dazlich, D. A., Los, S. O., … Jensen, T. G. (1996). Comparison of radiative and physiological effects of doubled atmospheric CO_2 on climate. *Science*, *271*(5254), 1402–1406. https://doi.org/10.1126/science.271.5254.1402

Seneviratne, S. I., Corti, T., Davin, E. L., Hirschi, M., Jaeger, E. B., Lehner, I., … Teuling, A. J. (2010). Investigating soil moisture-climate interactions in a changing climate: A review. *Earth Science Reviews*, *99*(3-4), 125–161. https://doi.org/10.1016/j.earscirev.2010.02.004

Shepherd, J., Caldeira, K., Haigh, J., Keith, D., Launder, B., Mace, G., … Watson, A. (2009). Geoengineering the climate - Science, governance and uncertainty (82 pp.) The Royal Society Policy.

Swann, A. L. S., Hoffman, F. M., Koven, C. D., & Randerson, J. T. (2016). Plant responses to increasing CO_2 reduce estimates of climate impacts on drought severity. *Proceedings of the National Academy of Sciences of the United States of America*, *113*(36), 10,019–10,024. https://doi.org/10.1073/pnas.1604581113

Teuling, A. J., Van Loon, A. F., Seneviratne, S. I., Lehner, I., Aubinet, M., Heinesch, B., … Spank, U. (2013). Evapotranspiration amplifies European summer drought. *Geophysical Research Letters*, *40*(10), 2071–2075. https://doi.org/10.1002/grl.50495

Tilmes, S., Fasullo, J., Lamarque, J.-F., Marsh, D. R., Mills, M., Alterskjær, K., … Watanabe, S. (2013). The hydrological impact of geoengineering in the Geoengineering Model Intercomparison Project (GeoMIP). *Journal of Geophysical Research: Atmospheres*, *118*, 11,036–11,058. https://doi.org/10.1002/jgrd.50868

Trenberth, K. E., & Dai, A. (2007). Effects of Mount Pinatubo volcanic eruption on the hydrological cycle as an analog of geoengineering. *Geophysical Research Letters*, *34*, L15702. https://doi.org/10.1029/2007GL030524

Wilhelm, M., Davin, E. L., & Seneviratne, S. I. (2015). Climate engineering of vegetated land for hot extremes mitigation: An earth system model sensitivity study. *Journal of Geophysical Research: Atmospheres*, *120*, 2612–2623. https://doi.org/10.1002/2014JD022293

Xia, L., Robock, A., Tilmes, S., & Neely, R. R. III (2016). Stratospheric sulfate geoengineering could enhance the terrestrial photosynthesis rate. *Atmospheric Chemistry and Physics*, *16*(3), 1479–1489. https://doi.org/10.5194/acp-16-1479-2016